Visual closed-loop dynamics via ocular drift

Liron Gruber and Ehud Ahissar

Department of Neurobiology, Weizmann Institute of Science, Rehovot 76100, Israel

Abstract

The human visual system perceives its environment via eye movements, which are typically classified as saccades and drifts. Saccades are quick transitions of the gaze from one Region of Interest (ROI) to another and drifts are slower scanning motions in each ROI. Here we examine two contrasting schemes of perception via these ocular movements: an open-loop computational and a closed-loop dynamical scheme. The two schemes entail contrasting predictions, specifically regarding the kinematics of ocular drifts and their dependency on concurrent visual inputs. We have thus designed an experiment in which measuring ocular kinematics while modulating the available visual information (controlled by image size and by a gaze-contingent display) can discriminate between the two schemes. Our results reveal that vision is a closed-loop dynamic process. This is demonstrated by (i) a dependency of the drift trajectory on the concurrent visual input (ii) condition-specific convergence of the drift speed within < 100ms (iii) periodic drift kinematics around 10 Hz and (iv) maintenance of selected motor-sensory "controlled variables". As these dynamics cannot be accounted for by an open-loop visual scheme, our results suggest that vision is inherently a closed-loop process, which dynamically and continuously links the brain to its environment.

Significance Statement

The visual system perceives its environment via eye movements, which are typically classified as saccades (quick transitions of the gaze from one region of interest, or ROI, to another) and drifts (slow scanning motions in each ROI). Two contrasting perceptual schemes might be consistent with this ocular movement pattern: a computational and a dynamical scheme. The two schemes, which obey open- and closed-loop dynamics, respectively, entail contrasting predictions regarding the kinematics of ocular drifts and their dependency on concurrent visual inputs. We tested these predictions by measuring ocular behavior while modulating the available spatial information (by reducing image size and by mimicking tunnel vision). We show that the behavior of the ocular drift is consistent with the dynamical, closed-loop scheme.

Introduction

The visual system perceives its environment via continuous eye movements. These movements can be primarily classified as saccades, which quickly (speeds between ~10 to ~1000 deg/s) shift the gaze from one ROI to another (1-3) and drifts, which slowly (speeds < ~10 deg/s) scan each ROI (4-7). Smooth pursuit, under this classification, results from the maintenance of fixation over a moving ROI. Saccades are often divided to macro and micro-saccades, shifting the gaze to targets beyond or within the foveal field, respectively. It is currently accepted that all saccades sit on the same kinematic continuum, controlled by the same circuits, and serve the same function – shifting the gaze to a new ROI (6, 8-11). Hence, here we analyze all saccades in one category.

Two contrasting perceptual schemes might be consistent with this saccade-drift pattern: an open-loop computational and a closed-loop dynamical scheme. In both schemes, saccades are controlled, at least in part, in a closed-loop manner in which ROI selection depends on the accumulated visual information (1, 2, 11-14). The two schemes, however, divide in their assumed acquisition process. The computational scheme assumes that at each ROI the visual system acquires one or more snapshots of the ROI and computes its internal

representation through an open-ended sequence of computations, much like in current computer-vision implementations (15-19). The dynamical scheme, in contrast, assumes that the acquisition of each ROI is a continuous closed-loop process, whose dynamics are determined by the interactions between the drift motion and the external image (20-25).

As a result, the two schemes entail contrasting predictions. The computational scheme predicts that the ocular drift will not depend on the concurrent visual input, whereas the dynamical scheme predicts that it will. The dynamical scheme further predicts that the drift will exhibit convergence or oscillatory dynamics during perception, as expected from the dynamics of a closed-loop system around its attractors (24); the computational scheme predicts that drift dynamics should follow a (presumably constant) predetermined or random pattern. Lastly, with closed-loops, adaptive changes are part of a process in which the values of a set of variables, the "controlled variables", are actively maintained within a certain range that allows the current functioning of the system (24, 26, 27). Open-loop systems do not have this active capacity and depend on a-priori mapping between environmental and internal variables.

To test the predictions of the two schemes, we measured ocular behavior while modulating the available spatial information by reducing image size and by mimicking tunnel vision. Briefly, we tracked subjects' gaze while they were scanning simple shapes of two sizes, and while revealing to them either the entire visual field ("natural viewing") or only a portion of the image around the center of the gaze ("tunneled viewing"). Using these real-time manipulations, we show that the ocular drift (i) depends on concurrent sensory data, (ii) dynamically converges to a condition-specific speed, (iii) converges anew after each saccade within < 100 ms and (iv) exhibits increased periodic activity around 10 Hz when vision is challenged. This behavior is not consistent with the open-loop scheme. Rather, it indicates that visual acquisition is a continuous dynamical process and further suggests that this dynamic process is accomplished within low-level retinal-neuronal-ocular loops. Consistent with this suggestion, the visual system maintained selected controlled variables across conditions, via a coordinated control of saccade-rate and drift kinematics. Importantly, part of the saccade-drift coordination occurred at the resolution of individual saccades.

Results

Five subjects were asked to identify an image on a screen as one of five options (square, rectangle, circle, triangle and a parallelogram) after viewing it either naturally or through tunneled viewing, during which spatial information was exposed only around the center of their continuously-tracked gaze. Two image sizes were presented (large, 10.80x10.80 deg; small, 0.90x0.90 deg) and two tunneling windows were used (2.90x1.90 deg for large images and 0.24x0.16 deg for small images). Success rates were 100% for natural viewing, 94±6% for the tunneled-large shapes and 60±2% for the tunneled-small shapes. Only correct trials were used for the analysis reported here.

Consistent with both perceptual schemes, limiting the available spatial information had a dramatic effect on the distribution of gaze centers. During natural viewing of large shapes, the gaze was typically directed to the center of the shape, while during tunneled viewing of large shapes the gaze was typically directed to the borders of the shapes (**Fig. 1a** and **Fig. S1a,b**). In fact, most (55±7%) of the saccades made by all subjects in all tunneled-large trials were border-following (**Fig. 1b**, see **Methods**). Strikingly, with tunneled viewing, saccades were directed along the image borders in a controlled manner (**Fig. 1b,c** and **Fig. S2)**.

While saccade planning could rely on information gathered in the preceding fixational pause, it could not rely on concurrent peripheral visual information (mean saccadic amplitude was significantly larger than window size, 3.45±0.07 vs 2.90 deg; $p<0.05$, n= 4648, one-tailed t-test; the large tunneling window is overlaid on the rectangle example in **Fig. 1a**). Saccadic border-following was evident already at the beginning of each trial and, on average, kept a constant profile along the trial (**Fig. 1d**), suggesting that saccade planning was indeed primarily based on the information collected during the immediately preceding fixational pause(s) rather than on an accumulated estimation of the object's shape.

We next examined the dependency of ocular kinematics on concurrent visual acquisition within each fixational pause. We first analyzed the instantaneous drift speed, i.e., the speed computed between two consequent eye recording samples (7). This calculation, which is

done on the raw unfiltered data, yields values that are typically higher than those obtained from filtered data are (**Fig. S3**). We refer to the former as representing the upper bounds (that include recording noise), and the latter as lower bounds (that filter out rapid movements), of the actual drift speed [a value not directly accessible to current tracking technologies (28, 29)]. For the sake of clarity, all comparisons across conditions are described primarily using the upper-bound data, assuming that the recording noise was similar across the different conditions.

The open-loop (computational) scheme predicts that ocular dynamics at each fixational pause will only depend on motor constrains. The closed-loop scheme predicts a dependency on real-time sensory information (24, 30). In all our conditions ocular drift speed exhibited a converging-like behavior; on average, the drift speed was strongly modulated at the beginning of each pause and gradually converged to an asymptotic value during the pause (**Fig. 2a**). The lower bound of the drift speed showed similar differences between target values (**Fig. S4f,g**), the drift speeds we measured did not depend on the pupil size or on the amplitudes or speeds of the saccades preceding them ($r^2 < 0.01$ for all cases), and these variables were not significantly different across viewing conditions (**Fig. S4**). The kinematics of the vertical and horizontal movements differed significantly (**Fig. S5a**); for example, with small images the horizontal movement did not differ between tunneled and natural viewing, while the vertical one did. These different dynamics likely indicate independent convergence dynamics within the vertical and horizontal sensory-motor loops during the first 100 ms of each pause. Comparing the dynamics of the two components later during the pause (**Fig. S5b**) with that of the combined motion in the horizontal-vertical plane (**Fig. 2a**, right panels) suggests that the convergence gradually became more coordinated between the vertical and horizontal loops as the fixational pause continued.

This ocular behavior did not reflect motor-only dynamics as the target-speed the eye converged to depended on the viewing condition, i.e., on sensory information. Yet, the dynamics here could result from a combination of a fast motor-only and slow sensory-motor dynamics. While the visual system had to converge to a given target speed anew in each fixational pause (**Fig. 2a**), the sensory-motor convergence on the appropriate value of

the target speed could be accomplished slowly across trials within each block, as viewing conditions were constant per block (see **Methods**).

A sensory variable that did change on a pause-by-pause basis was the presence of an image-border in the visual field. Comparisons of the mean drift speeds revealed that indeed the mean drift speed per pause (*Sp*) depended on the presence of a border in the ROI - *Sp* was significantly lower when drifting along borders than otherwise in all conditions [4.6±0.2 versus 5.1±0.1 deg/s (n=1686 and 4124 pauses, respectively), $p<0.05$, two-tailed t-test]. We further analyzed the scanning patterns during pauses and found that during pauses that were close to borders, drift trajectories scanned the image differently if vision was challenged or not. When challenged by tunneling or a small image size, the eye tended to drift in a curvier pattern (31) when scanning a border, remaining closer to their starting location. The distributions of curvature indexes (see **Methods**) differed between border and non-border drifts in both tunneled conditions ($p<0.05$, Kolmogorov–Smirnov test), and the mean curvature index differed in all conditions ($p<0.05$, two-tailed t-test) except for the natural-large condition ($p=0.7$) (**Fig. 2c**). Thus, the speed and trajectory of ocular drift in each pause depended on the actual visual data available at that pause.

If a fast sensory-motor loop is active, repetitive dynamics may emerge in individual pauses. We thus analyzed the periodic behavior of ocular drifts in all conditions. Following (32) we computed the autocorrelations of the drift separately for the vertical and horizontal instantaneous velocities. Consistent with (32), we found a substantial amount of oscillating drifts and more so in the vertical direction. The primary oscillating frequency in all these cases was ~10 Hz, which nicely fit the sensitivity profile of many sensory spatiotemporal channels (33). The fraction of significantly-oscillating drifts at 10 Hz was significantly larger in tunneled versus natural conditions (**Fig. 3**, 38.3% vs 12.8% in the vertical direction; $\chi^2=18.5$,dof=1, $p<0.005$).

The results described so far indicate a closed-loop sensory-motor behavior of the visual system and suggest that the closed-loop processing is done at multiple levels. What may the visual system try to maintain using these loops, and specifically during natural and tunneled perceptual epochs? To address these questions, we analyzed the averaged kinematics in each condition. In all subjects, both saccade average rate (*Rs*) and mean drift

speed per pause (*Sp)* increased in tunneled conditions compared to natural viewing of small images; this was also the case for 3 of the 5 subjects when viewing large images (**Fig. 4a,b; Table S1).** Assuming that visual information is acquired during fixational pauses (12, 34-37) and that photoreceptors are activated by illumination changes, the mean rate of visual acquisition (during a pause) should be proportional to *Sp* (5, 38) and the amount of visual information collected during that pause should be proportional to the integrated distance scanned by the eye (the length of its trajectory) during the pause ($Xp = Sp / Rs$).

Importantly, the tunneling-induced changes in *Rs* and *Sp* compensated each other keeping *Xp* unchanged, on average, for each stimulus size (**Table 1**). Thus, when tunneled, the visual system appeared to increase the ROI sampling rate (*Rs*) while maintaining *Xp* and compromising (i.e., loosening) the control of *Sp*; evidence for such loosening of control can be found in the increased variance of *Sp* during tunneled viewing (**Fig. 4c**). Interestingly, a different strategy appeared with size changes. When viewing small sized images, the visual system decreased the ROI sampling rate while maintaining *Sp* and thus compromising the control of *Xp* (**Fig. 4a,b, Table 1**). A sequential open-loop scheme, in which the visual input affects *Rs and Rs* affects the drift variables, is ruled out here; the mean values of *Rs* did not systematically change along with either *Sp* or *Xp* (**Table 1)** and the pause-by-pause correlations between each *Sp* or *Xp* and its preceding instantaneous *Rs* (i.e., the inter-saccadic-interval) were negligible ($R^2 < 0.06$).

If the visual system maintains *Sp* across image sizes and compromises its control when challenged with tunneling, then the trial-to-trial variability of *Sp* should reflect that. Indeed, while *Sp* exhibited relatively small coefficients of variation (CVs) during natural viewing (0.90 and 0.57 for large and small, respectively), its CVs increased significantly when tunneled (1.22 and 1.02 for large and small, respectively; **Fig. 4c; Table S1**). Interestingly, the kinematics of the saccadic jumps, which are often considered open-loop ballistic movements, also appeared to be under certain (likely low-level) closed-loop control; while obeying a main-sequence pattern to the same extent in natural and tunneled conditions for low saccadic amplitudes (amplitudes that scaled with the image size - up to 7.5 deg for large and 3 deg for small images); saccade kinematics showed higher variations beyond these amplitudes in tunneled vision (**Fig. S5**).

Discussion

Consistent with previous reports (5, 32, 39-41), our results demonstrate clearly that ocular drifts are actively controlled by the visual system. What our results add is that this control is part of a closed-loop process - drift kinematics, which affect the visual input, depend on this input. We demonstrate this closed-loop behavior via five major observations. First, we showed that the trajectory of the drift in the ROI depends on the concurrent sensory data. When the drift scanned an image border its scanning trajectory was controlled to be slower and curvier than when it scanned a non-border ROI (**Fig. 2b-e**). Second, we showed that the drift speed dynamically converges to a condition-specific speed; even when starting with the same speed, the visual system gradually changed its drift speed until it converged to a value that was specific to the viewing condition (**Fig. 2a**). Third, we showed that the system converges to its target speed anew after each saccade within < 100 ms on average (**Fig. 2a**). Such a rapid convergence can only be achieved in loops who's cycle time is smaller than the convergence time – in the visual system these are low-level [certainly sub cortical; (42)] loops. Forth, we showed that the drift speed exhibits periodic oscillations around 10 Hz (**Fig. 3**). Such oscillations can be produced by either 10 Hz pace makers, not observed so far in the drift control system, or by closed loops whose cycle time, again, is smaller or equal to 100 ms. Fifth, both convergence dynamics and oscillatory patterns were different for the vertical and horizontal components of eye movements (**Figs. S5** and **3**, respectively). This observation rules out a general broad activation profile during fixational pauses and supports an independent convergence processes in the vertical and horizontal retino-neuro-muscular loops (43) during pause initiation. As mentioned above, these loops gradually become more coordinated as the pause continues.

These results do not rule out additional contributions to drift control, other than those of the concurrent visual input, such as experience- and context-dependent biases (5, 32, 40) or slow motor-control processes (44). Under the closed-loop framework, these broader and slower contributions would operate within higher-level sensory-motor loops (11, 24).

Our measurements are contaminated with measurement noise. With video-based methods, such as the one we used, the major noise sources are inaccurate calibration and changes in the pupil size and head movements (45, 46). As our results are based on comparisons

between conditions measured with the same method, we ruled out the possibility that the differences we found stemmed from differences in pupil size (see Results) and insufficient calibration (we calibrated the device before each trial – see Methods). We could not rule out head movements as a possible additional source of slow kinematics [head movements most likely cannot account for the rapid kinematics demonstrated in **Fig. 2a** (47, 48)]. It is important to note, however, that since head movements always contribute to retinal image-motion (4, 39, 48, 49) their isolation is not required for testing whether visual acquisition is obtained via open- or closed-loop dynamics – head movements are part of these dynamics.

Our data suggest that under normal conditions the visual system controls its drift speed such as to maintain it within a specific range [see also (30)]. One plausible reason for such a control is to maintain temporal coding relatively constant at a range suitable for neural processing (11, 29, 50, 51). When viewing small-size images the visual system does not compromise this control and even tightens it (**Fig. 4c**), possibly for increasing the reliability of sensory data. However, when challenged with tunneled viewing, which decreases the amount of available spatial information, the system compromises the control of drift speed, allowing its increase, for maintaining constant scanning distances under an increased rate of ROI switching (shorter fixational pauses), thus increasing total spatial information on the expense of its reliability (**Table 1**). Thus, saccadic ROI switching, which is controlled by both global scene- and task-related factors (1, 2, 6, 10, 52-54) and local ROI-specific factors (6, 11), appears to be controlled in coordination with the control of the ocular drift (**Fig. 5a**). We further show here that this coordination is manifested in real time on a cycle-by-cycle basis (**Fig. 1**).

In our paradigm, the coordinated saccade-drift control maintained, on average, *Sp* across image sizes in natural viewing, and *Xp* across viewing conditions (**Fig. 5b**). The identification of these controlled variables was possible only at the population level, and not with individual subjects. This is not surprising, given the complexity of the human visual system and its need to cope with many changing conditions in life. These results, thus, suggest that *Sp* and *Xp* are controlled in most of the individual subjects in the manner described above, as part of a larger set of idiosyncratic controlled variables.

That visual information is acquired continuously along each fixational pause had been demonstrated previously (12, 34-37). Our results now provide substantial evidence that this acquisition is accomplished by retino-neuro-oculo closed-loops, involving low (certainly subcortical) levels of the visual system. Together with the known closed-loop basis of ROI selection, our results now suggest that vision is inherently a closed-loop process. That is, that all visual processing components are accomplished within brain-environment closed-loops (**Fig. 5**). As such, the distinction between "early" and "late" processes cannot be appropriate for visual perception. Rather, the system appears to rely on unceasingly working lower and higher closed-loop processes that continuously interact.

How visual perception emerges from such closed-loop processes is not clear yet. What appears to be essential components of closed-loop visual perception, judging from the behavioral level addressed here (55), are the steady-state attractors of the visual brain-environment loops (24). Being inherently a closed-loop system does not preclude the ability of the visual system to perceive a certain amount of information even when eye movements are prevented, as often occurs in the laboratory. Being a closed-loop system simply entails, in this context, that every movement of the eye is a component of visual perception and that the system continuously attempts to converge to its attractors, getting as close to a given attractor as possible, given the collection of internal and external constrains.

Methods:

Subjects. 5 healthy subjects with normal vision at the ages 21-28 participated in the experiments (3 females, 2 with right dominant eye, 3 with left dominant eye). All subjects were given detailed explanation about the eye tracker device and the behavioral task, and were paid for their participation. Informed consents were obtained from all subjects, in accordance with the approved Declaration of Helsinki for this project.

Experimental Setup. The experiment took place in a darkened and quiet room where subjects sat in front of a high-resolution, fast computer screen (VPixx, 1920x1080, 120Hz). The movements of the dominant eye were recorded at 100Hz (EyeLink II) while the other

eye was blindfolded. Subjects sat 1 meter away from the screen and placed their chin on a chinrest to reduce head movements.

Stimuli and gaze windows. Two kinds of images were created: 'large' and 'small', and each was associated with a specific gaze window – a horizontal rectangle centered on the subject's gaze at each sample and through which the image was exposed. The large shapes occupied 10.80±0.15x10.80±0.15 deg (720±10x720±10 pixels), and the large gaze window was 2.90±0.15x1.90±0.15 deg (190±10x130±10 pixels). The small shapes occupied 0.90±0.03x0.90±0.03 deg (60±2x60±2 pixels) with a gaze window of 0.24±0.03x0.16±0.03 deg (13±2x9±2 pixels). The ratio between image and window size was the same for both image sizes (**Videos S1, S2**).

Experimental Design. We tested the performance of subjects in a five forced choice shapes recognition tasks. In each trial, one out of five filled gray basic shapes against a black background was presented (square, rectangle, circle, triangle and a parallelogram; see **Fig. 1**). These images were presented in two forms, large and small, as described above. Subjects were tested during 5 days. During days 1-3 they performed 2 tunneled vision sessions, the first one with large images and the second one with small images. On day 4 they performed two additional tunneled vision sessions with small images. On day 5 they performed 4 sessions of natural viewing, 2 repetitions with each image size: large, small, large, and small. Each tunneled trial lasted up to 30 s, mean trial duration for tunneled large was 9+2 s and for tunneled small 20+4 s (trials with natural viewing lasted 3 s, hence all comparative analyses were further verified using only the first 3 s of all tunneled trials, to control for trial length confounds, **Table S1**). There were at least 2 repetitions of each shape in each session (10-12 trials per session, only the first two repetitions of each shape were used for analysis), and hence each session lasted up to 12 minutes. Before the beginning of each trial the eye tracker was recalibrated (46). We used an adaptive calibration method: subjects fixated on a '+' and waited until the gaze report of the eye tracker (marked as 'X') stabilized. The error between the two markers was used to correct the eye tracker's output during the next trial. At the end of each trial subjects reported which of the five shapes was presented, and received a 'correct/wrong' feedback. In the tunneled vision sessions, subjects had to identify a shape that was "hidden" on the screen and exposed only through

the gaze window (see above). In the natural vision sessions, subjects had to identify the same shapes, naturally viewing them with no constrains.

Eye movement processing. A velocity based algorithm [modified from Bonneh et al. (56)] was used for detecting all saccades and drift. We used the following threshold parameters for saccades detection: 16 deg/s minimal peak velocity and 0.3 deg minimal amplitude. Each detected saccade was visually examined to verify the quality of saccadic detection. Fixation periods between saccades were labeled drift only if they lasted > 30 ms. Upper bounds of the instantaneous drift speed were computed as the derivative of the raw eye position signal. Lower bounds were computed as derivatives of the filtered signals [a third order Savitzky-Golay filter with window size of 3 samples (31)]. For **Fig. S1** we in addition used saccadic detection threshold parameters of 3 deg/s for minimal peak velocity and 0.05 deg for minimal amplitude, in order to match previous publications (31).

Borders analysis. Border-following movements during tunneled viewing were those movements in which the border of the shape was visible to the subject during the movement. This was determined by the window size: saccades or drift pauses that started and ended at less than 1.8 deg (for large), or 0.15 deg (for small) from a border, were classified as "border saccade" or "border drift", respectively. During natural viewing border-following movements were defined using the same distance criteria.

Curvature index. We defined an index for drift curvature, $c = \frac{Xp-Dp}{Xp+Dp}$ where Xp equals the length of the drift trajectory and Dp equals the linear distance between its starting and ending points. Hence, c=0 represents a straight line and c=1 represents a closed curve.

Statistical analyses. Two-tailed t-tests were used to evaluate the significance of differences in the mean values of kinematic variables (*Rs*, *Sp*, *Xp*, *c*), all of which exhibited normal distribution for all subjects. N's for *Rs* statistics in tunneled-large, natural-large, tunneled-small, natural-small, respectively, were: Subj1 (30,19,30,20); Subj2 (29,20,30,19); Subj3 (27,20,28,18); Subj4 (30,20,30,19); Subj5 (25,20,30,20); N's for *Sp* and *Xp* statistics were (respectively): Subj1 (1756,229,2392,154); Subj2 (534,110,2626,45); Subj3 (723,129,2108,101); Subj4 (409,104,1288,46); Subj5 (1085,203,2775,136).; The distributions of c values were also compared using two-sample Kolmogorov-Smirnov tests.

Variances were compared via the corresponding coefficients of variation (CV = variance/mean), using two-sample F-tests. Data are expressed as mean ± S.E.M. Shape presentation order was randomized using a uniform distribution. No blinding was done during analysis and none of the data points was excluded.

Data availability Statement. All analyses were done using MATLAB. All data is available upon request.

Acknowledgements: We thank Amos Arieli for his invaluable help in performing the experiments and Michele Rucci and Rafi Malach for commenting on earlier versions of the manuscript. This research was supported by the European Research Council (ERC) under the European Union's Horizon 2020 research and innovation programme (grant agreement No 786949). E.A. holds the Helen Diller Family Professorial Chair of Neurobiology.

Author contributions: L.G. conducted the experiments and analyzed the data. L.G. and E.A. conceived the project, designed the experiments and wrote the paper.

Competing interests: The authors declare no competing financial interests.

References

1. Noton D & Stark L (1971) Scanpaths in eye movements during pattern perception. *Science* 171(968):308-311.
2. Yang SC-H, Lengyel M, & Wolpert DM (2016) Active sensing in the categorization of visual patterns. *Elife* 5.
3. Meermeier A, Gremmler S, & Lappe M (2016) The influence of image content on oculomotor plasticity. *Journal of vision* 16(8):17-17.
4. Steinman RM & Levinson JZ (1990) The role of eye movement in the detection of contrast and spatial detail. *Eye Movements and Their Role in Visual and Cognitive Processes*, ed Kowler E (Elsevier, Amsterdam), pp 115-212.
5. Rucci M & Victor JD (2015) The unsteady eye: an information-processing stage, not a bug. *Trends in Neurosciences* 38:195-206.
6. Krauzlis RJ, Goffart L, & Hafed ZM (2017) Neuronal control of fixation and fixational eye movements. *Phil. Trans. R. Soc. B* 372(1718):20160205.
7. Ahissar E, Ozana S, & Arieli A (2015) 1-D Vision: Encoding of Eye Movements by Simple Receptive Fields. *Perception* 44(8-9):986-994.

8. Zuber BL, Stark L, & Cook G (1965) Microsaccades and the velocity-amplitude relationship for saccadic eye movements. *Science* 150(3702):1459-1460.
9. Rolfs M, Kliegl R, & Engbert R (2008) Toward a model of microsaccade generation: The case of microsaccadic inhibition. *Journal of vision* 8(11):5.
10. Ko HK, Poletti M, & Rucci M (2010) Microsaccades precisely relocate gaze in a high visual acuity task. *Nature neuroscience* 13(12):1549-1553.
11. Ahissar E, Arieli A, Fried M, & Bonneh Y (2014) On the possible roles of microsaccades and drifts in visual perception. *Vision research* 118:25-30.
12. Wolf C & Schütz AC (2015) Trans-saccadic integration of peripheral and foveal feature information is close to optimal. *Journal of vision* 15(16):1-1.
13. Shen K & Paré M (2014) Predictive Saccade Target Selection in Superior Colliculus during Visual Search. *The Journal of Neuroscience* 34(16):5640-5648.
14. Friston K, Adams R, Perrinet L, & Breakspear M (2012) Perceptions as hypotheses: saccades as experiments. *Frontiers in Psychology* 3.
15. Crick FHC, Marr DC, & Poggio T (1981) An information-processing approach to understanding the visual cortex. *The organization of the cerebral cortex*, ed Schmitt FO (MIT Press, Cambridge), pp 505-533.
16. Treisman AM & Gelade G (1980) A feature-integration theory of attention. *Cognit Psychol* 12(1):97-136.
17. Pitkow X, Sompolinsky H, & Meister M (2007) A neural computation for visual acuity in the presence of eye movements. *PLoS Biol* 5(12):e331.
18. Poggio T & Serre T (2013) Models of visual cortex. *Scholarpedia* 8(4):3516.
19. Cadieu CF*, et al.* (2014) Deep neural networks rival the representation of primate IT cortex for core visual object recognition. *PLoS computational biology* 10(12):e1003963.
20. Uexkull Jv (1926) *Theoretical biology* (K. Paul, Trench, Trubner & co. ltd, London).
21. Powers WT (1973) Feedback: beyond behaviorism. *Science* 179(71):351-356.
22. Van Gelder T & Port RF (1995) It's about time: An overview of the dynamical approach to cognition. *Mind as motion: Explorations in the dynamics of cognition* 1:43.
23. Kelso JS (1997) *Dynamic patterns: The self-organization of brain and behavior* (MIT press).
24. Ahissar E & Assa E (2016) Perception as a closed-loop convergence process. *eLife* 5:e12830.
25. Saig A, Gordon G, Assa E, Arieli A, & Ahissar E (2012) Motor-sensory confluence in tactile perception. *The Journal of Neuroscience* 32(40):14022-14032.
26. Marken RS (2009) You say you had a revolution: Methodological foundations of closed-loop psychology. *Review of General Psychology* 13(2):137.
27. Buckley CL & Toyoizumi T (2018) A theory of how active behavior stabilises neural activity: Neural gain modulation by closed-loop environmental feedback. *PLoS computational biology* 14(1):e1005926.
28. Fang Y, Gill C, Poletti M, & Rucci M (2018) Monocular microsaccades: Do they really occur? *Journal of vision* 18(3):1-14.
29. Rucci M, Ahissar E, & Burr D (2018) Temporal coding of visual space. *Trends in cognitive sciences* 22(10):883-895.
30. Biswas D*, et al.* (2018) Closed-Loop Control of Active Sensing Movements Regulates Sensory Slip. *bioRxiv*:366609.
31. Cherici C, Kuang X, Poletti M, & Rucci M (2012) Precision of sustained fixation in trained and untrained observers. *Journal of vision* 12(6):31.
32. Herrmann CJ, Metzler R, & Engbert R (2017) A self-avoiding walk with neural delays as a model of fixational eye movements. *Scientific Reports* 7(1):12958.

33. Burr DC, Ross J, & Morrone MC (1986) Seeing objects in motion. *Proc. R. Soc. Lond. B. Biol. Sci.* 227:249-265.
34. Burr DC (1981) Temporal summation of moving images by the human visual system. *Proc.R.Soc.Lond.B.Biol.Sci.* 211:321-339.
35. Watt R (1987) Scanning from coarse to fine spatial scales in the human visual system after the onset of a stimulus. *JOSA A* 4(10):2006-2021.
36. Rucci M, Iovin R, Poletti M, & Santini F (2007) Miniature eye movements enhance fine spatial detail. *Nature* 447(7146):851-854.
37. Grill-Spector K & Kanwisher N (2005) Visual recognition: As soon as you know it is there, you know what it is. *Psychological Science* 16(2):152-160.
38. Ahissar E & Arieli A (2001) Figuring space by time. *Neuron* 32:185-201.
39. Martinez-Conde S, Macknik SL, & Hubel DH (2004) The role of fixational eye movements in visual perception. *nature reviews neuroscience* 5(3):229-240.
40. Rolfs M (2009) Microsaccades: small steps on a long way. *Vision research* 49(20):2415-2441.
41. Kagan I (2012) Active vision: fixational eye movements help seeing space in time. *Current biology : CB* 22(6):R186-188.
42. Schmolesky MT*, et al.* (1998) Signal timing across the macaque visual system. *Journal of neurophysiology* 79(6):3272-3278.
43. Sparks DL (2002) The brainstem control of saccadic eye movements. *Nature Reviews Neuroscience* 3(12):952.
44. Kowler E & Steinman RM (1979) The effect of expectations on slow oculomotor control. I. Periodic target steps. *Vision research* 19(6):619-632.
45. Drewes J, Zhu W, Hu Y, & Hu X (2014) Smaller is better: Drift in gaze measurements due to pupil dynamics. *PloS one* 9(10):e111197.
46. Nyström M, Andersson R, Holmqvist K, & Van De Weijer J (2013) The influence of calibration method and eye physiology on eyetracking data quality. *Behavior research methods* 45(1):272-288.
47. Skavenski A, Hansen R, Steinman RM, & Winterson BJ (1979) Quality of retinal image stabilization during small natural and artificial body rotations in man. *Vision research* 19(6):675-683.
48. Poletti M, Aytekin M, & Rucci M (2015) Head-eye coordination at a microscopic scale. *Current Biology* 25(24):3253-3259.
49. Gilchrist ID, Brown V, & Findlay JM (1997) Saccades without eye movements. *Nature* 390(6656):130-131.
50. Ahissar E (1998) Temporal-code to rate-code conversion by neuronal phase-locked loops. *Neural Comput.* 10(3):597-650.
51. Ahissar E & Arieli A (2012) Seeing via miniature eye movements: A dynamic hypothesis for vision. *Frontiers in Computational Neuroscience* 6:89.
52. Yarbus AL (1967) *Eye Movements and Vision* (Plenum, New York).
53. Findlay JM & Brown V (2006) Eye scanning of multi-element displays: II. Saccade planning. *Vision research* 46(1-2):216-227.
54. Schütz AC, Braun DI, & Gegenfurtner KR (2011) Eye movements and perception: A selective review. *Journal of vision* 11(5):9-9.
55. Krakauer JW, Ghazanfar AA, Gomez-Marin A, MacIver MA, & Poeppel D (2017) Neuroscience needs behavior: correcting a reductionist bias. *Neuron* 93(3):480-490.
56. Bonneh YS*, et al.* (2010) Motion-induced blindness and microsaccades: cause and effect. *Journal of vision* 10(14):22.

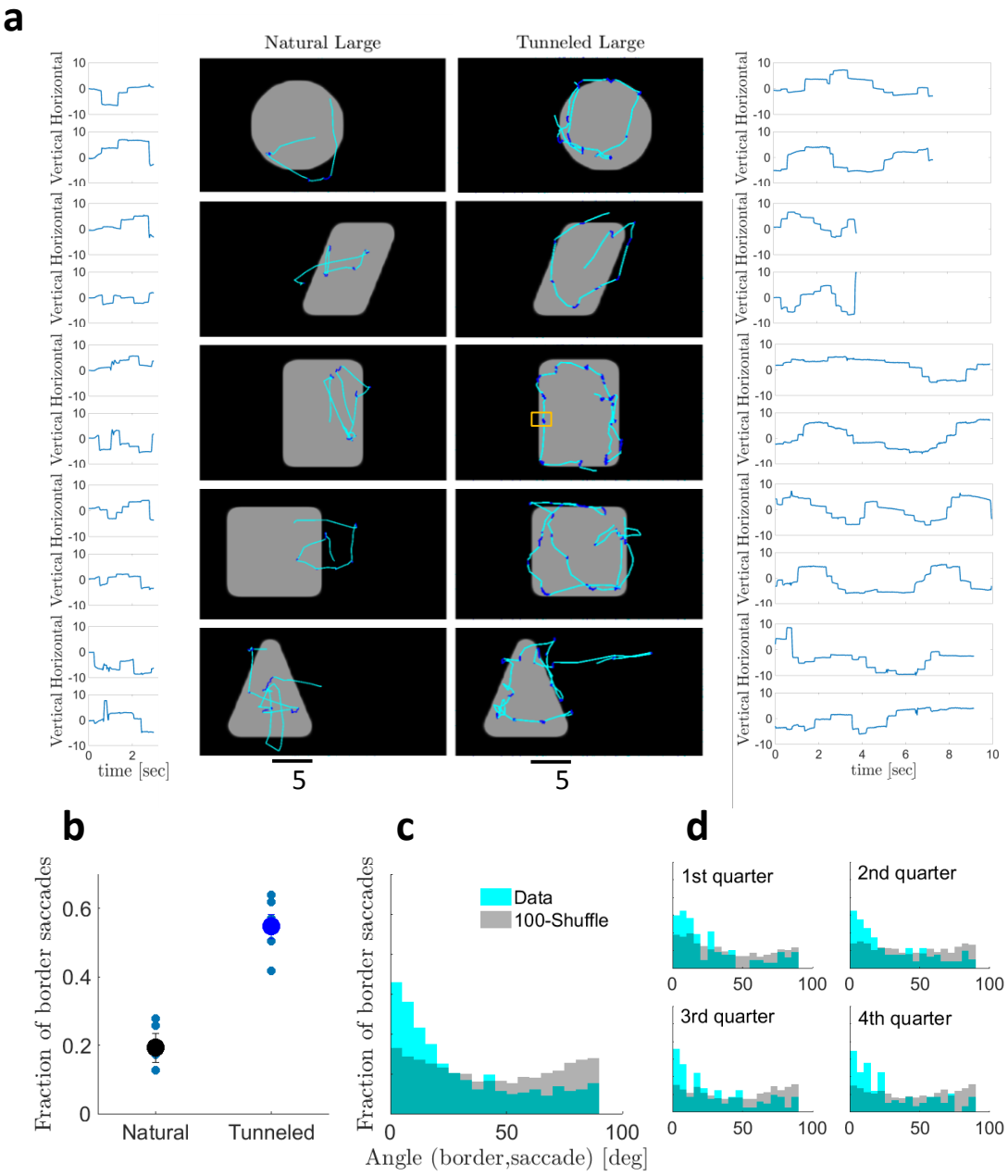
a
Natural Large
Tunneled Large
Vertical Horizontal
time [sec]
5
5
b
Fraction of border saccades
Natural
Tunneled
c
Data
100-Shuffle
Fraction of border saccades
Angle (border,saccade) [deg]
d
1st quarter
2nd quarter
3rd quarter
4th quarter

Figure 1. Eye trajectories. (a) Example of eye trajectories in single trials with natural (left) and tunneled (right) large viewing. Saccades, lighter blue; fixational pauses, dark blue; traces, horizontal and vertical components as a function of time next to each example (movies of these examples are in **Videos S3-S7**). **(b)** Fractions of border-following saccades in the two large conditions for each subject (small dots) and their means (large colored dots). **(c)** Distribution of the angles between the orientation of the border scanned during a pause and the direction of the immediately following saccade with tunneled large viewing [data shown in light blue, shuffled data (saccade directions were shuffled before angle computation; average of 100 repetitions is depicted) in gray; the two histograms are superimposed in the graph]. Analyses of individual subjects are presented in **figure S2**. **(d)** Same as (c) for the first, second, third and fourth quarter of each trial.

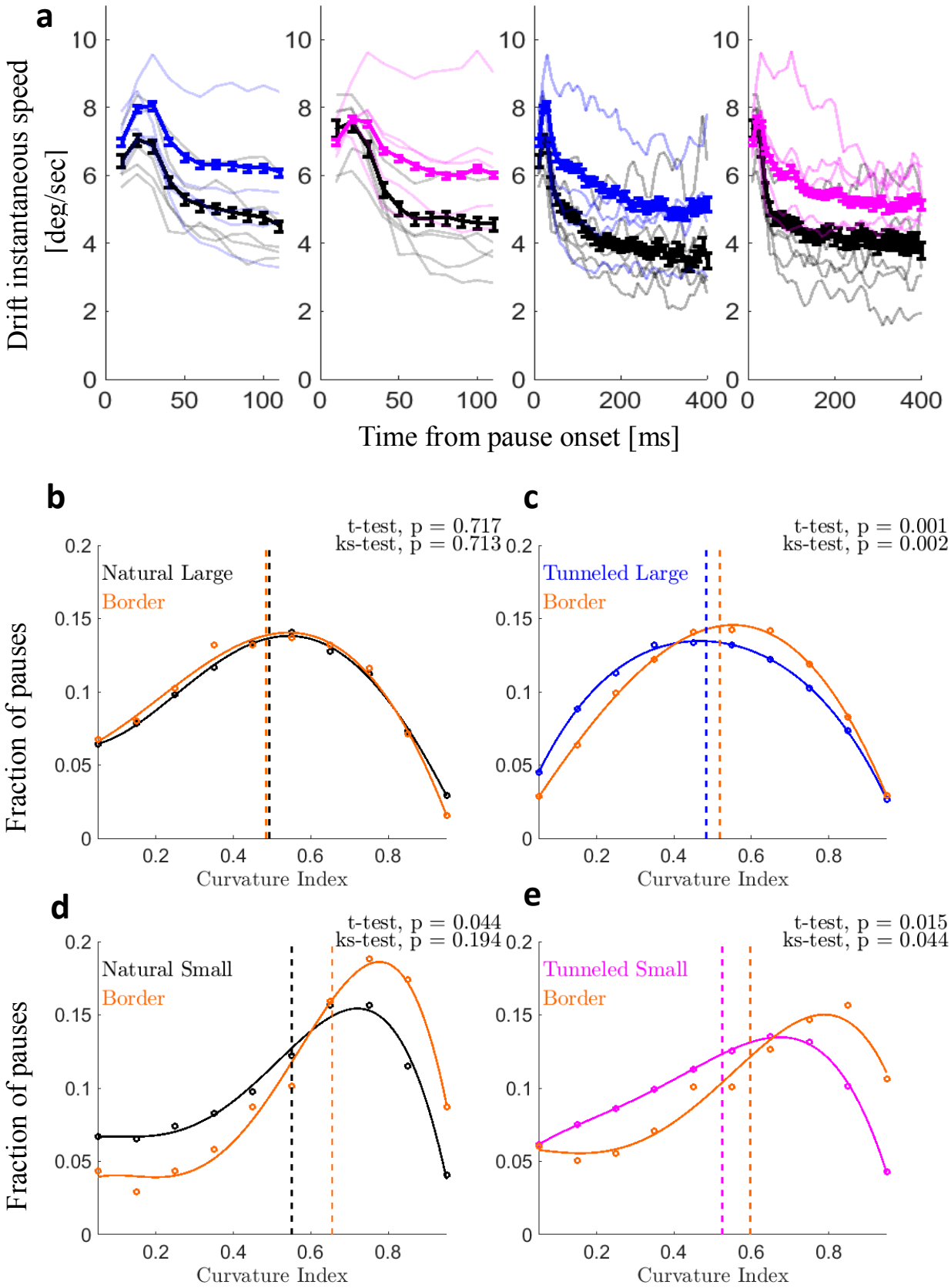
a
Drift instantaneous speed [deg/sec]
Time from pause onset [ms]
b
t-test, p = 0.717
ks-test, p = 0.713
Natural Large
Border
Fraction of pauses
Curvature Index
c
t-test, p = 0.001
ks-test, p = 0.002
Tunneled Large
Border
Curvature Index
d
t-test, p = 0.044
ks-test, p = 0.194
Natural Small
Border
Fraction of pauses
Curvature Index
e
t-test, p = 0.015
ks-test, p = 0.044
Tunneled Small
Border
Curvature Index

506

Figure 2. Instantaneous drift speed and curvature indices. **(a)** Mean within-pause instantaneous drift speeds presented for large (1st & 3rd plot) and small objects (2nd & 4th plot), depicted in two time scales. Light-color traces depict the dynamics in individual subjects. Natural viewing in black and tunneled viewing in color (large in blue and small in magenta); error-bars denote SEMs across pauses. **(b-e)**. Distributions of curvature indices (see Methods) of border drift trajectories (brown) and non-border drifts, in the four experimental conditions. The vertical dashed lines depict the mean values of curvature indices across all pauses and subjects per condition. Mean ± SEM and number of pauses for border and non-border scanning, respectively: 0.48±0.04 vs. 0.49±0.01 for natural-large (n=192,374 pauses); 0.52±0.01 vs. 0.48±0.01 for tunneled-large (n=1405,757); 0.65±0.05 vs. 0.55±0.02 for natural-small (n=23,270); 0.60±0.03 vs. 0.53±0.01 for tunneled-small (n=66,2723); p-values in each panel are for (i) comparing means using two tailed t-tests and (ii) comparing distributions using two-sample Kolmogorov-Smirnov tests.

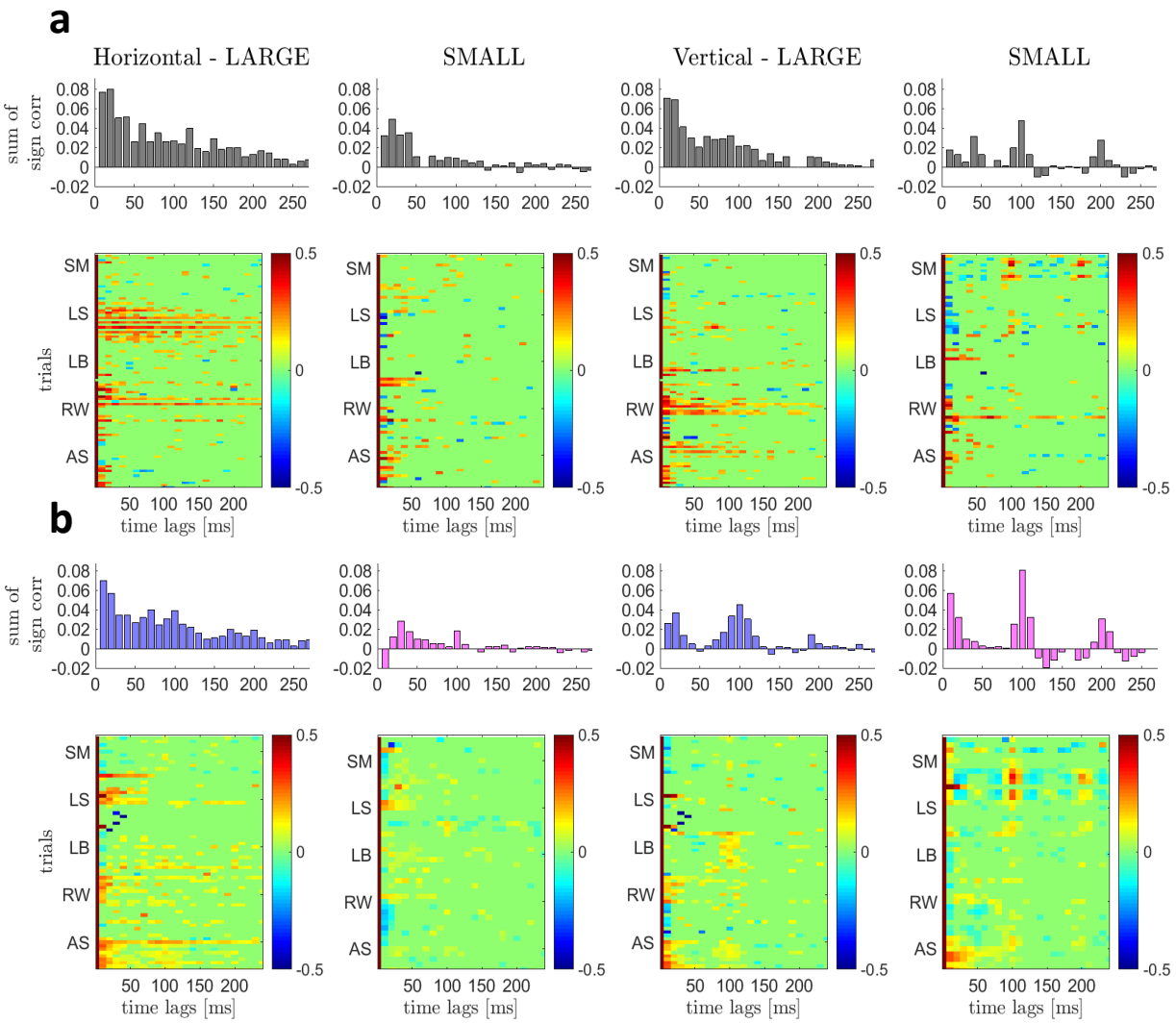

534

535

536

537

538

539

Figure 3. Patterns of significant autocorrelations of the instantaneous drift speed. (a) Patterns of significant correlations of the horizontal and vertical instantaneous drift speed in the natural viewing condition. Autocorrelations were calculated per trial, from the data recorded during all fixational pauses of that trial. Significance values were computed for each time lag using confidence bounds of 2 STD. The upper row shows, for each time lag, the mean correlation value of all significant correlations across all subjects and trials. The lower row presents the correlation values of all significant time lags in all trials; the values of non-significant lags were zeroed. Subjects' initials are depicted at left, at the middle of their relevant trial rows. **(b)** Same as (a) for the tunneled viewing tasks.

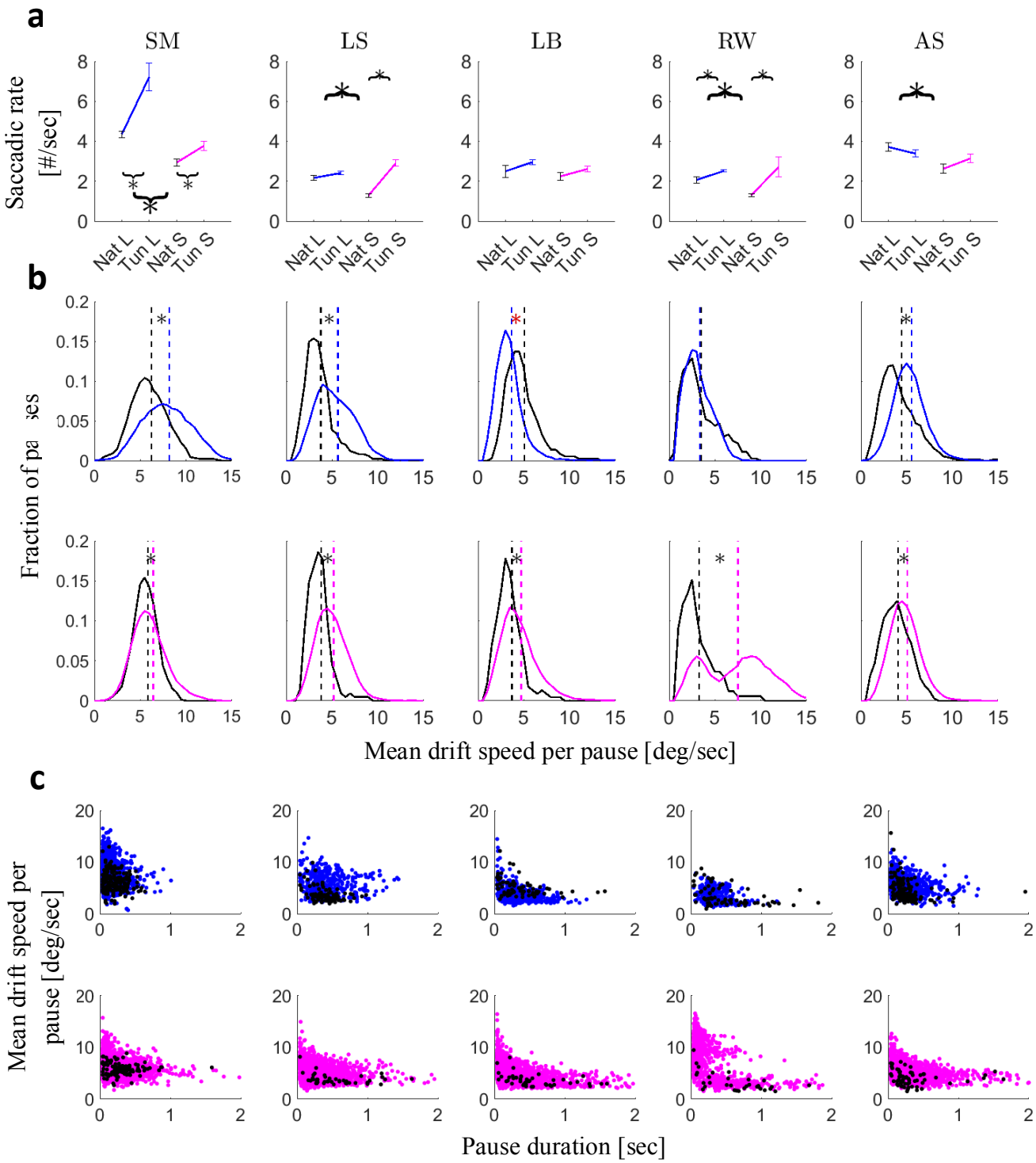
a
SM
LS
LB
RW
AS
Saccadic rate [#/sec]
Nat L
Tun L
Nat S
Tun S
b
Fraction of pa ses
Mean drift speed per pause [deg/sec]
c
Mean drift speed per pause [deg/sec]
Pause duration [sec]

Figure 4. Kinematics of saccades and drifts. (a) Changes in mean saccadic rates (*Rs*) between natural and tunneled viewing for large (blue) and small (magenta) image sizes. Data for each subject (left) and their mean (right most) are presented (*, $p<0.05$, two tailed t-tests). **(b)** Distributions of the mean upper bounds of instantaneous drift speeds per pause (*Sp*) in the four experimental conditions; data presented as in (a) (*, $p<0.05$, two tailed t-tests, red asterisk marks a subject who showed a reversed effect). **(c)** Mean drifts speeds versus pause durations in the four experimental conditions. N's for *Rs* statistics in tunneled-large, natural-large, tunneled-small, natural-small, respectively, were: Subj1 (30,19,30,20); Subj2 (29,20,30,19); Subj3 (27,20,28,18); Subj4 (30,20,30,19); Subj5 (25,20,30,20); N's for *Sp* and *Xp* statistics were (respectively): Subj1 (1756,229,2392,154); Subj2 (534,110,2626,45); Subj3 (723,129,2108,101); Subj4 (409,104,1288,46); Subj5 (1085,203,2775,136).

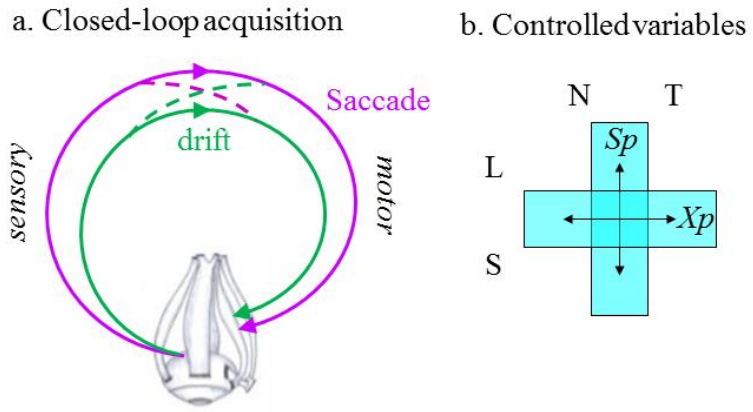

Figure 5. Closed-loop visual acquisition. (**a**) Coordinated saccade and drift closed-loops. The two loops interact with each other, coordinating the control of the acquisition controlled-variables. (**b**) Controlled variables. The scheme symbolizes the maintenance of *Sp* across image size (large and small) and the maintenance of *Xp* across viewing conditions (natural and tunneled).

Mean values of kinematic variables

	Sp	***Xp***	***Rs***
NL	4.89±0.09	1.33±0.04	2.9±0.1
TL	5.81±0.05	1.40±0.04	3.7±0.2
NS	4.56±0.09	1.77±0.08	2.0±0.1
TS	5.60±0.03	1.63±0.08	3.0±0.1

Table 1. Mean values of kinematic variables. Mean ± SEM of visual scanning variables during each viewing condition (NL, natural large; TL, tunneled large; NS, natural small; TS, tunneled small). *Sp* is the mean instantaneous drift speed during a pause in deg/s, *Xp* is the distance travelled during a pause in deg and *Rs* is the mean saccadic rate per trial. Green arrows indicate values that do not differ statistically ($p > 0.15$); all other differences were statistically significant ($p < 0.05$, two tailed t-tests).